INFLUENCE OF A TURBULENCE CONTROL SCREEN ON THE AERODYNAMIC AND AEROELASTIC BEHAVIOR OF A UHBR FAN

Alexandra Schneider, Benoît Paoletti, Xavier Ottavy, Christoph Brandstetter

INFLUENCE OF A TURBULENCE CONTROL SCREEN ON THE AERODYNAMIC AND AEROELASTIC BEHAVIOR OF A UHBR FAN

Alexandra P. Schneider [1], Benoit Paoletti [1], Xavier Ottavy [1], Christoph Brandstetter*[1]

[1] Université de Lyon, École Centrale de Lyon, CNRS, LMFA, UMR 5509, F-69134, ECULLY, France

ABSTRACT

A composite fan stage representative of a modern Ultra High Bypass Ratio (UHBR) architecture has been investigated experimentally on a novel test facility at Ecole Centrale de Lyon.

For these experiments, a turbulence control screen (TCS), a hemisphere, consisting of honeycomb and wiremesh panels, was installed in front of the rig in order to ensure homogeneous, disturbance-free inflow conditions. This kind of screen was developed in the early 1970 years to investigate flight-noise on static test beds. Today, they are commonly used in aero-engine and fan tests, because they improve the accuracy of acoustic measurements and provide more reproducible performance tests.

However, the influence of such screens has been investigated only from an acoustic point of view in the past. This study presents a back-to-back comparison of measurements with and without the TCS, which allows a characterization of the effects on aerodynamic and aeroelastic behavior of the fan stage. The investigation was carried out for multiple stable operating points on two different speed lines to obtain a global image of the influence at part and design speed. The utilization of steady and unsteady instrumentation in different axial and circumferential duct positions allows a detailed analysis of similarities and differences of the configuration without and with the TCS and provides insight into underlying physical mechanisms.

INTRODUCTION

In the early 1970 years it was recognized that the radiated noise of aircraft engine fans shows much higher tonal noise levels (i.e. the amplitudes of the blade passing frequency (BPF) and its higher harmonics in the acoustic spectra are higher) in static tests compared to in-flight tests [1, 2, 3]. This leads to the fact that flight noise levels were typically overpredicted when static test beds were used for acoustic characterization of new aircraft engines or fans.

Analytical and experimental studies proved that these higher BPF levels were caused by an interaction of rotor blades with inflow distortions or atmospheric turbulence [4, 5, 6, 1, 2]. (Unsteady) velocity disturbances cause varying angles of attack when the blades are passing through them. This results in unsteady lift forces, which work as a dipole source and hence radiate random noise [6].

Under static test conditions velocity disturbances caused by atmospheric turbulence are stretched in the streamwise direction as they are sucked into the engine intake. At the same time they are contracted in the directions perpendicular to the main flow direction forming elongated vortical structures with a length that can exceed multiple rotor diameters. These structures are chopped several times by the rotor blades and are hence quasistationary disturbances in the non-rotating frame of reference i.e. periodic disturbances in the rotating frame of reference. This results in narrow band frequency peaks around the BPF and its higher harmonics [6, 1, 3]. The comparison of in-flight, windtunnel and static tests showed that these disturbances are reduced with forward speed producing BPF peaks with lowered amplitudes under flight conditions [7, 8].

In order to reduce the discrepancy between static and in-flight acoustic tests several research institutes started to develop so-called turbulence control screens (TCS, or inflow control device, ICD) [9, 10, 8, 11, 12]. These structures, typically consisting of honeycomb panels and/or wire-mesh screens, were placed upstream of the fan rotor in form of planar screens [3] or with a hemispherical [10, 8] or geodesic shape [12] in order to ensure homogeneous inflow conditions. Acoustic and aerodynamic investigations of these structures showed a significant reduction of inflow turbulence intensities and therefore lowered BPF amplitudes and peak widths (especially at subsonic operating conditions) while broadband noise levels stayed nearly unchanged

*Corresponding author: christoph.brandstetter@ec-lyon.fr

[3,9,10,8,11,12,13,14,15,16]. This allows to simulate in-flight noise radiation on static test beds which is much less cost intensive than acoustic characterization in fly-over tests.
Since these early studies the use of TCS to simulate in-flight noise radiation under static test conditions was accepted and many test facilities for acoustic investigations of fans or aircraft engines are equipped with such structures ([17,18,19,20,21,22, 23,24]). However, in most of the mentioned studies the influence of the TCS is analyzed only from an acoustic point of view. The results of the back-to-back comparisons of the facility with and without TCS presented in literature confirm the findings mentioned above. At subsonic blade tip speeds BPF amplitudes were significantly reduced if the facility is operated with TCS while at supersonic tip Mach numbers the influence of the TCS on the acoustic spectra is small. Broadband noise levels are hardly affected by TCS for all operating conditions [20,25,21,24,26]. In addition, novel mode decomposition methods yield that no additional propagating modes were introduced due to the use of TCS and that cut-on modes can be stabilized (i.e. they are more prominent in the spectra) through TCS [24,26].
Besides a detailed acoustic characterization Caldas et al. [24] investigated the flowfield upstream of the rotor via hot-wire anemometry. They found a reduction of the averaged turbulence intensity from 1.8% to 0.3% as well as lower fluctuation of the axial velocity over the channel height if the TCS is used in the experiments. A decomposition of turbulence intensity levels into different frequencies is not presented.

There is lack in literature about the influence of a TCS on the flowfield in the rotor plane and on the mechanical behavior of the rotor. In the case of slender, lightweight composite rotor blades this information is crucial due to the high sensitivity of the blades to changes in aerodynamics. Especially near the stability limit the susceptibility to blade vibrations rises and small inflow disturbances can trigger safety-critical vibration amplitudes or the onset of rotating stall if they interact with the rotor blades.

At the test facility ECL-B3 at Ecole Centrale de Lyon (ECL), used for investigations of UHBR fan stages, a hemispherical TCS is usually installed in front of the intake for acoustic and performance measurements. According to established procedures at ECL, operability measurements are usually conducted without TCS.
In order to make results of both configurations comparable to each other and provide information for design of experiments (DoE) procedures for future measurement campaigns, it is necessary to study the influence of the TCS in detail. Salze et al. [27] already analyzed acoustic spectra from measurements with and without TCS. These measurements have been carried out within the project ENOVAL at the test facility ECL-B3 (see also [28]) and allowed the validation of TCS for acoustic experiments.

Based on that, this study presents a more detailed back-to-back comparison of both configurations to allow a characterization of the influence of the TCS on the aerodynamic and aeroelastic behavior of the fan stage. It is analyzed if higher inflow disturbances, which appear without TCS, result in a higher instationarity of the flow field and hence higher fluctuations of aerodynamic flow features like the shock at transonic operating conditions. Besides that, the study focuses on the effect of the TCS on the stable operating range i.e. the influence on stall onset and potentially safety-critical synchronous and non-synchronous blade vibrations.

In order to overcome the lack of information in literature concerning the effect of a TCS on characteristic flow features such as broadband turbulence, inflow distortion and mechanical behavior of the rotor, this study aims to provide more insight in the aerodynamic and aeroelastic influence of a TCS. Therefore this paper is structured as follows:

· The experimental setup is introduced including the different probe positions used within this study. The overall fan performance is shown for two investigated speedlines.
· The inflow conditions of the rotor stage are characterized for both measurement configurations.
· At design speed the influence of the TCS on rotor steady and unsteady aerodynamics is discussed for different operating conditions. Furthermore the effect on structure mechanics and the aeroelastic coupling between rotor flow and blade vibrations is analyzed in detail.
· The results of the design speed line are completed by the analysis of blade tip flow and related blade vibrations at part speed in order to obtain global trends for the whole operating range.

TEST FACILITY ECL-B3

The test facility ECL-B3 was designed and built in cooperation between ECL and Safran Aircraft Engines through the ANR-EQUIPEX program. It is used for investigations of fan architectures representative of modern UHBR stages at scales around 1:4. The stage investigated within this study consists of a composite, low speed transonic fan and Outlet Guide Vanes (OGV), designed by Safran AE. The latter have been designed specifically for this rig in order to provide the rotor with representative exit conditions without separation of core and bypass stream.

Setup

The ECL-B3 test rig presented in Fig. 1 was built to enable highly accurate aerodynamic and acoustic characterization of the vehicle, such as the modern UHBR fan rotor used for the studies in this paper. The test vehicle is placed in an anechoic chamber, acoustically isolated from the machine room, which hosts a 3MW electric motor allowing a rotational speed of up to 16000rpm. A torquemeter is mounted between the fan shaft and the gearbox shaft enabling an accurate measurement of the applied power. The rig is operated in an open cycle, thus air is sucked in through traversing rows of silencers on the roof before it enters the core section. Subsequently the air flows into

an axisymmetric coned shaped throttle controlling the massflow before exiting through an exhaust system and a final row of silencers to atmosphere. The Venturi nozzle within the 25 m long circular pipe of the exhaust system allows precise massflow measurements.

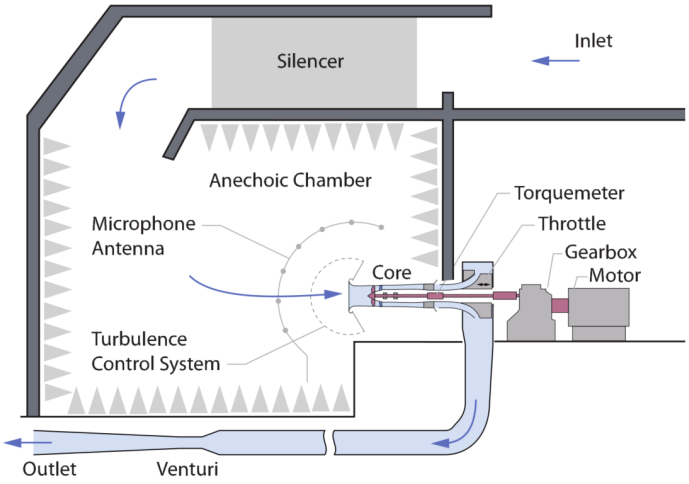

FIGURE 1: SCHEMATIC VIEW OF ECL-B3 TEST FACILITY

To ensure homogeneous, disturbance-free inflow conditions a Turbulence Control Screen (TCS) is installed in front of the core section for acoustic and performance measurements. This sphere with a diameter of about 2 m consist of wiremesh and honeycomb panels in order to reduce the incoming turbulence and inflow distortions (Fig. 2).

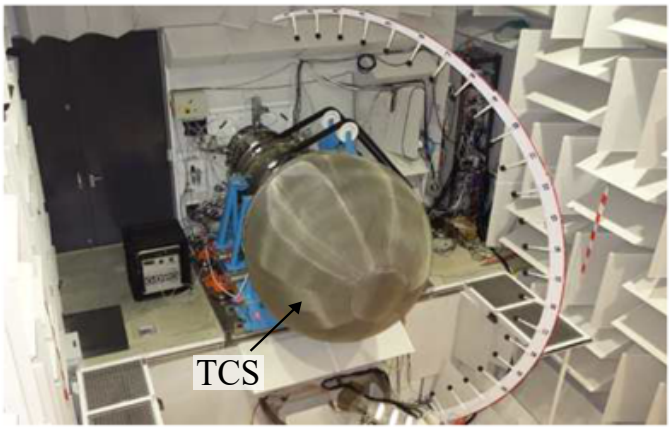

FIGURE 2: ECL-B3 TEST FACILITY WITH TURBULENCE CONTROL SCREEN

The main parameters of the investigated fan stage are summarized in Table 1.

TABLE 1: MAIN PARAMETERS OF UHBR FAN STAGE

Outer casing diameter	508 mm (20”)
Rotor number of blades	16
Stator number of blades	36
Design Blade Tip Speed	280-340 m/s
Design Tip gap size	$\sim 0.8\%$ tip chord

Test procedure

The ENOVAL aerodynamic test campaign consisted in two maneuvers: the fan mapping measurements, with full traversals of the stage exit plane at stable operating conditions, and the operability measurements during which the machine was throttled towards the stability limit. The latter will be investigated in detail within this study.

To characterize the influence of the TCS, measurements with the sphere in front of the facility (screen configuration) will be compared to measurements without it (open configuration). Several stable operating points at two different speedlines are used for this back-to-back comparison.

Instrumentation

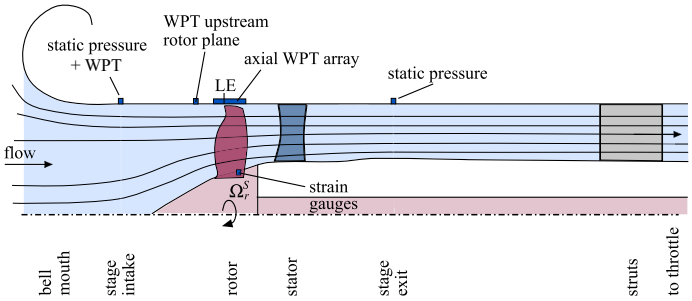

FIGURE 3: SCHEMATIC VIEW OF THE MACHINE CORE AND PROBE POSITIONS

The machine core schematized in Fig. 3 was designed in a modular fashion granting a time-efficient and flexible change of test configuration. It also facilitates the application of instrumentation, as multiple accesses are available for traversable instrumentation around the circumference. The acquisition system allows more than 800 signals to be recorded simultaneously. The machine core is instrumented with pressure and temperature sensors as well as microphones distributed from the bellmouth shaped intake to the throttle mechanism at various meridian positions, on the hub and casing.

Besides flush-mounted static pressure probes, miniature

high frequency response wall pressure transducers (WPT) are placed in various axial and circumferential positions in order to observe unsteady aerodynamics in the machine. The measurement of structural vibrations was implemented through blade-mounted strain gauges on the rotor, transferred via telemetry (see [29] for details).

Fan performance map

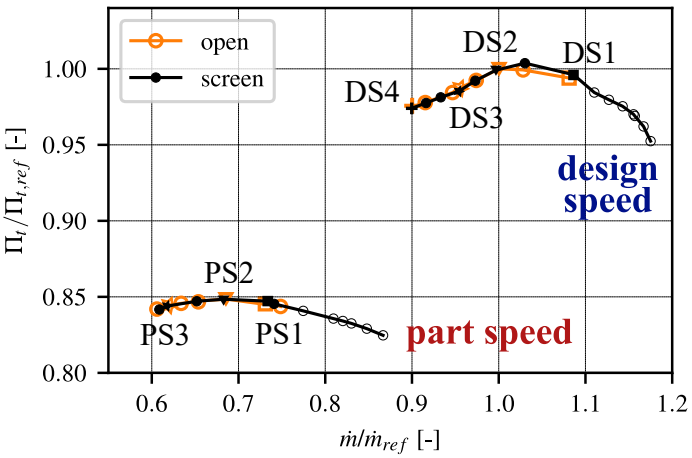

FIGURE 4: FAN PERFORMANCE MAP AND INVESTIGATED OPERATING POINTS

The fan performance map shown in Fig. 4 is obtained by reducing the massflow through different settings of the outlet throttle for two different speed lines. As mentioned above, this procedure leads to slightly differing operating conditions (shifted massflows) between both configurations. In order to enable a better classification of the investigated operating points of the operability measurements, those of the fan mapping measurements (for the configuration with the TCS) are shown in Fig. 4 as well (unfilled black dots).

In Fig. 4 it is visible, that the characteristics for both configurations show a similar total pressure ratio over a wide range of massflow. In addition, the stall margin is nearly identical for both configurations for the shown part and design speed line.

As indicated by the marked operating points in Fig. 4, four approximately equally spaced operating points of the operability measurements will be used for a detailed comparison of the screen and the open configuration at design speed in section *DESIGN SPEED*. For the analysis of the part speed behavior three operating points OP_{PS1} to OP_{PS3} will be discussed in section *PART SPEED*.

Before this detailed investigation of different operating points, the inflow conditions will be characterized for both configurations in the following section. For this characterization the operating point OP_{DS1} and an operating point with a rotational speed near design speed will be used.

INFLOW CONDITIONS

Based on the literature cited in the introduction above, it is assumed that inflow inhomogeneity and unsteadiness are reduced, if the TCS is installed in front of the facility. In order to analyze the influence of the TCS on the inflow conditions of the fan stage, static pressure probes and WPTs upstream of the rotor plane (see Fig. 3) are used in this section to characterize the flow field in this region.

The unsteadiness of the flow field upstream of the rotor can be analyzed by regarding the static pressure time fluctuations (pressure at a given sensor position $p_{s,i}$ minus time average indicated by $\overline{(\cdot)}$ over the whole measurement time), normalized with the dynamic inlet pressure

$$\Delta p_{rel,i} = \frac{\Delta p_{s,i}}{p_{dyn,i}} = \frac{p_{s,i} - \overline{p_{s,i}}}{p_{t,in} - \overline{p_{s,i}}} \tag{1}$$

of static pressure probes in varying circumferential positions i in the stage intake (see Fig. 5). For the comparison of both con-

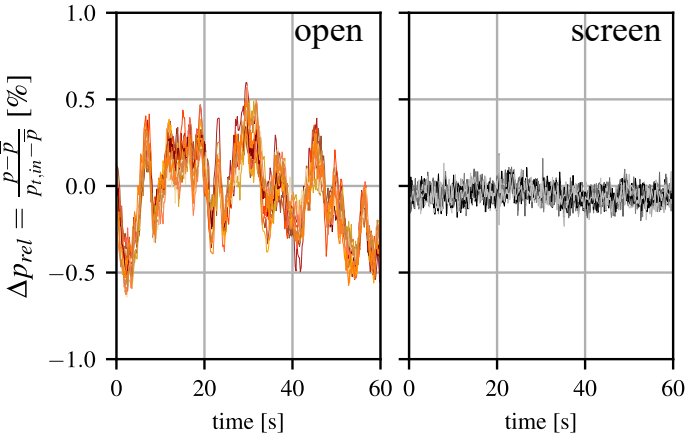

FIGURE 5: TEMPORAL STATIC PRESSURE FLUCTUATION IN STAGE INTAKE AT OP_{DS1} (DESIGN SPEED) FOR 12 CIRCUMFERENTIALLY DISTRIBUTED SENSORS, FLUCTUATION REPRESENTATIVE FOR ALL STUDIES OPERATING POINTS

figurations the signals for operating point OP_{DS1} during a measurement time of one minute (sampling frequency $= 5\,\mathrm{Hz}$) are used. These curves are qualitativly representative for all operating points at design and part speed. Fig. 5 shows static pressure fluctuations of up to 0.6 % of the dynamic inlet pressure for the open configuration. These fluctuations are related to large scale, aerodynamic fluctuations with characteristic timescales, resulting in circumferentially coherent variations of the static pressure. These structures can therefore be assumed to be quasistationary in the non-rotating frame of reference and can be considered as a slow and homogeneous variation of the fan operating conditions. For the screen configuration static pressure fluctuations are within about $0.1\,\% p_{dyn}$ significantly lower as for the open configuration. This indicates a strong reduction of the global unsteadiness of the flow field due to the TCS.

To investigate the inhomogeneity (circumferential asymmetry) of the flow field upstream of the rotor, Fig. 6 presents the circumferential profile of the static pressure for both configurations (0° corresponds to the 12h position). This graph shows the local temporal average of the wall pressure $\overline{p}(\theta)$, recorded at stable operating conditions using sensors traversed around the circumference and normalized with the dynamic pressure ($\widetilde{(\cdot)}$ here indicates an average over all circumferential positions):

$$p_\theta = \frac{\overline{p}(\theta) - \widetilde{\overline{p}(\theta)}}{\overline{p}_{t,in} - \widetilde{\overline{p}(\theta)}} \tag{2}$$

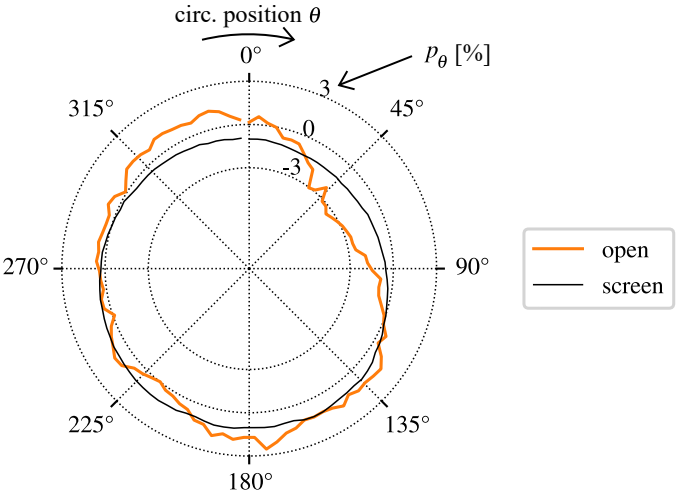

FIGURE 6: FLUCTUATION OF LOCAL TEMPORAL AVERAGE OF WALL PRESSURE FROM TRAVERSED WPTS UPSTREAM OF ROTOR PLANE NEAR DESIGN SPEED

From Fig. 6 it is evident that the static pressure varies about $\pm 2.5\,\% p_{dyn}$ around the circumference for the open configuration. If the TCS is installed, this variation is reduced to about $\pm 1\,\% p_{dyn}$, which leads to a more homogeneous inflow. Besides that, it is remarkable that the static pressure distribution for the screen configuration resembles a sinusoidal signal, whereas it is more complex in the case of the open configuration. While the sinusoidal pattern corresponds to a circumferential mode order of one, the strong pressure gradient in the pattern of the open configuration is realized through a superposition of different, higher mode orders.

This relation becomes even more obvious by regarding Fig. 7, which shows the spatial Fourier Transformation (FT) of the circumferential pressure profiles p_θ presented in Fig. 6. It is clearly visible that the circumferential pressure distribution of the screen configuration contains mainly a single mode order. In contrast, the FT of the open configuration depicts a composition of the pressure profile of mode order 1 and 2 with nearly equal amplitudes as well as higher mode orders with lower amplitudes. This proves that the TCS reduces not only the unsteadiness of the inflow, but also the circumferential inhomogeneity. The remaining circumferential asymmetry with mode order 1, which is present even if the TCS is installed, can be explained by the geometry of the facility chamber. As stated in the *SETUP* section, air is sucked in from the roof what results in a quasi-stationary, non-uniform flow field upstream of the stage intake. This non-uniformity is smoothed through the TCS but can not be completely homogenized.

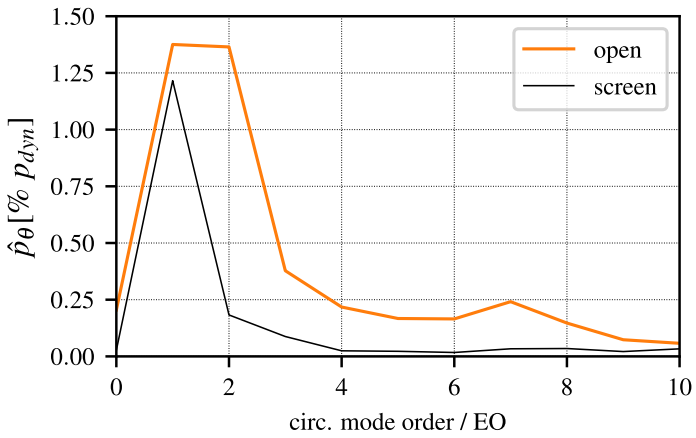

FIGURE 7: MODE DECOMPOSITION OF STATIC PRESSURE DISTRIBUTION p_θ UPSTREAM OF ROTOR PLANE NEAR DESIGN SPEED

In addition to the global unsteadiness of the flow field, analyzed in Fig. 5, the local unsteadiness (i.e. local, temporal fluctuations of the unsteady pressure, which is calculated by subtracting an ensemble average of 10 rotor revolutions, see eq. (1) in [29]) can be characterized by the standard deviation

$$\sigma_\theta = \frac{\sigma\left(p_{unsteady}(t)\right)(\theta)}{\overline{p}_{t,in} - \widetilde{\overline{p}(\theta)}} \tag{3}$$

of the unsteady pressure $p_{unsteady}(t)$. Fig. 8 shows this parameter, normalized with the dynamic pressure, depending on the circumferential position for both configurations. It becomes visible that the local unsteadiness for the open configuration fluctuates between 4 % and 6.2 % around the circumference. In contrast to that, it varies only marginally between 2.8 % and 3.3 % for the screen configuration. This results in higher spatial gradients and an increased average unsteadiness over the whole circumference in the open case.

Thus, the local flow unsteadiness strongly varies without application of the TCS. Fig. 6 and 8 indicate that the local turbulence level and the local average flow conditions, at which the fan operates around the circumference are inhomogeneous for the open configuration. This clearly explains increased tonal noise emissions, as it has been observed by Salze et al. [27], due to unsteady loading. The results from Fig. 5 additionally indicate a slowly fluctuating operating condition of the fan in the open case.

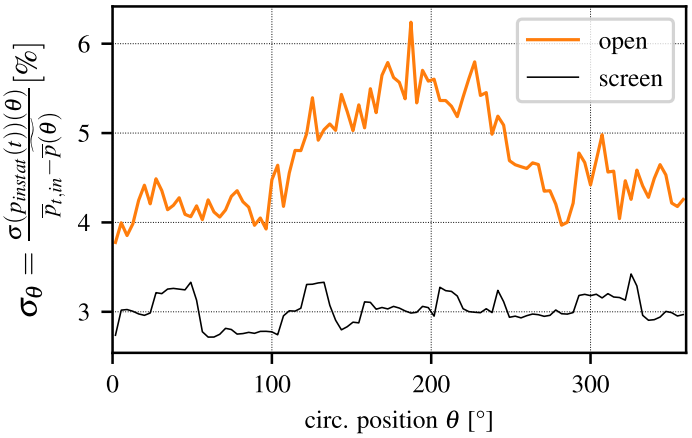

FIGURE 8: LOCAL, TEMPORAL STATIC PRESSURE FLUCTUATIONS σ_θ UPSTREAM OF ROTOR PLANE NEAR DESIGN SPEED

The figures presented in this section highlight the differences in inflow conditions between the configurations with and without TCS. Confirming results from literature, the TCS reduces global and local, temporal and spatial pressure fluctuations and gradients and therefore ensures a more homogeneous flow field upstream of the rotor.

DESIGN SPEED

In this section the effect of the different inflow conditions, which have been identified in the previous section, on aerodynamic and aeroelastic properties will be investigated in detail at four stationary operating points (as presented in Fig. 4) at the design speedline.

Ensemble averaged flow structure

The flow field in the rotor tip region can be visualized by using the axial WPT array above the rotor blades (Fig. 9a)), which is located at a circumferential positon of 336° (indicated in Fig. 6). This means that Fig. 9a) represent the flow field, which is observed by a sensor at a distinct circumferential position during the time of one rotor revolution and not the circumferential pattern at a given point in time. The presented flow fields are obtained by ensemble averaging the signal of each sensor over 100 rotor revolutions and are shown for the screen configuration. Shocks are clearly visible for all operating points in Fig. 9a) due to a sharp pressure rise upstream of the LE. This shock results from transonic flow over the blade's suction side in the rotor tip region and indicates transonic operating conditions at design speed. The reduction in massflow from OP_{DS1} to OP_{DS4} leads to lower axial velocities and in consequence to a reduced relative suction side velocity. Hence, shock strength is decreased from OP_{DS1} to OP_{DS4}. In addition, the shock is shifted upstream i.e. away from the LE, when the back pressure rises due to closing of the outlet throttle. The flow pattern becomes highly asymmetric around the circumference (in the rotating frame of reference) at throttled operating points. While the flow field is nearly identical

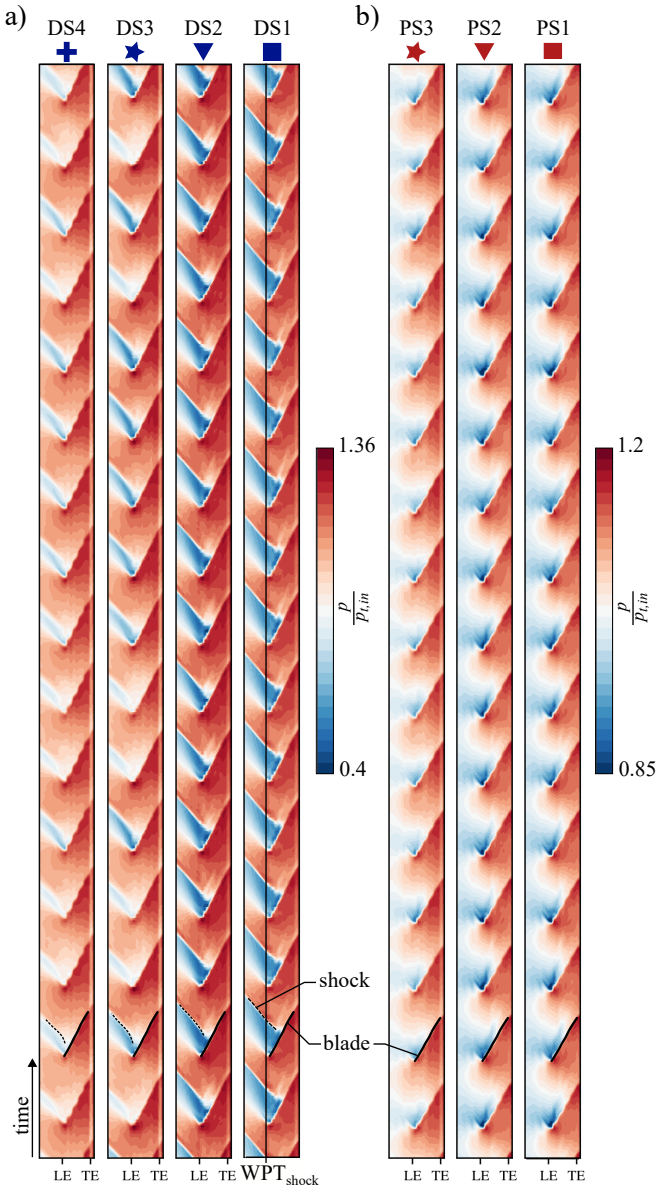

FIGURE 9: ENSEMBLE AVERAGED FLOW FIELD AT ROTOR TIP (FROM AXIAL WPT ARRAY AT 336°) FOR THE SCREEN CONFIGURATION: a) DESIGN SPEED; b) PART SPEED

for all blade passages at OP_{DS1} and OP_{DS2} it shows significant differences between adjacent channels at OP_{DS3} and OP_{DS4}.
The flow fields for the corresponding operating points for the open configuration are not shown here, due to the high similarity between both configurations.
Fig. 9b) shows the pressure field for the part-speedline, indicating purely subsonic operation and homogeneous passage flow for all blades. This stands in contrast to the transonic speed, which develops severe and blade-to-blade asymmetry for throttled conditions.

A detailed comparison of the aeordynamics of both config-

urations at the blade tip is enabled by Fig. 10, which shows the signal of the WPT directly upstream of the LE for OP_{DS2}, OP_{DS3} and OP_{DS4}. OP_{DS1} is similar to OP_{DS2} and omitted for brevity. According to the results presented in Fig. 9a), the signal has been ensemble averaged over 100 rotor revolutions in order to remove temporal fluctuations. Thus, Fig. 10 visualizes the ensemble averaged shock position and strength of the 16 channels.

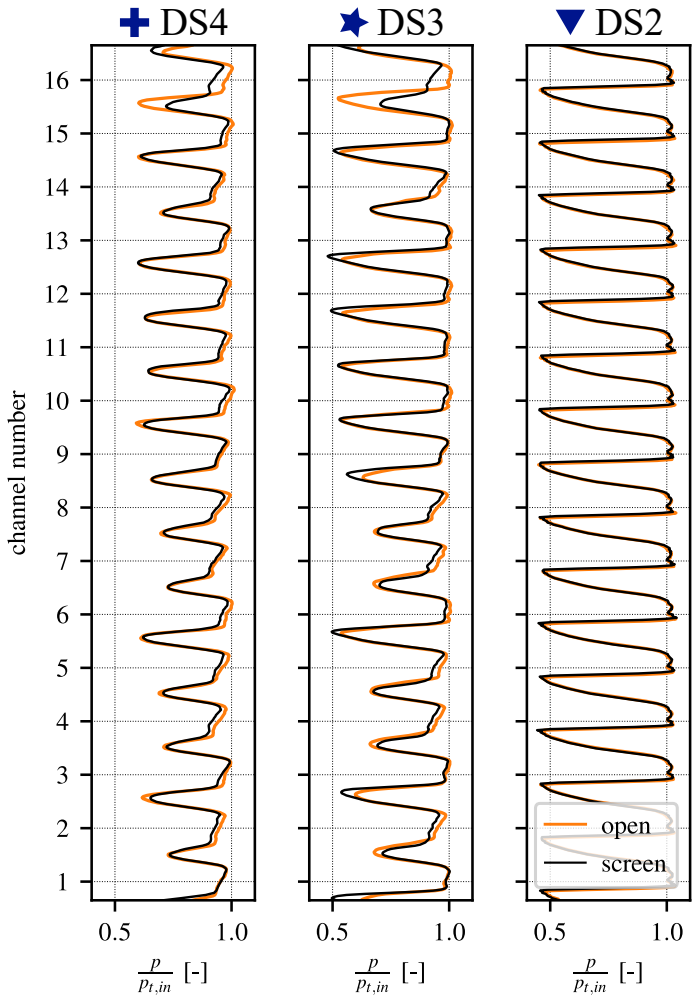

FIGURE 10: EVOLUTION OF THE ENSEMBLE AVERAGED FLOW ASYMMETRY WITH ROTOR THROTTLING AT DESIGN SPEED (WPT IN AXIAL ARRAY UPSTREAM OF LE USED)

Fig. 10 confirms that the shock is shifted upstream and the shock strength is reduced if the rotor is throttled. These trends can be observed for both configurations and the shock position in the passage is nearly identical in both cases at all presented operating points.

At the unthrottled operating point OP_{DS2} the shock position and strength is highly symmetric around the circumference. The detailed comparison of both configurations reveals slightly lower shock strengths for the open configuration compared to the screen configuration at this operating point.

If the massflow is reduced from OP_{DS2} to OP_{DS3}, a distinct asymmetry pattern evolves, which results in strongly varying shock strength around the circumference. Comparing the signals of the open configuration to these of the screen configuration, a strong difference in channel 15 can be noticed. For the open configuration the shock strength of this channel is only marginally reduced due to rotor throttling, whereas it significantly decreases in the screen case. In addition, the overall asymmetry is slightly weaker for the open configuration at OP_{DS3}, i.e. the difference between strong and weak shocks is smaller than for the screen configuration (the standard deviation is reduced by about 3%).

A further reduction in massflow to OP_{DS4} leads to a change in absolute shock strength, but has no influence on the asymmetry pattern. This means that the channels with a reduced shock strength are identical for OP_{DS3} and OP_{DS4} and that the discrepancy of shock strength in channel 15 between both configurations remains high. Besides that, only minor differences between open and screen asymmetry pattern are visible at OP_{DS4}, which are negligible compared to differences in shock strength around the circumference.

Thus, it is concluded that the TCS has, apart from channel 15, no influence on the observed asymmetry pattern and that this pattern is a rotor characteristic and stationary in the rotating frame of reference. Wilson et al. [30] and Lu et al. [31] describe blade untwist as responsible for inhomogeneous shock patterns at unloaded conditions, but near the stability limit, the presented resolution of the flow field has not been reported in literature and seems to be specific for low-speed composite fans. In a previous study at the same test facility but with a different rotor, Brandstetter et al. [32] have shown that the fan assembly developed an asymmetric shock pattern in a similar way, which correlated with the geometry variability of the blades, but assumed, that started flow conditions are prevalent in individual blades. The results presented here show that all shocks remain detached from the leading edge. It is intended to use Tip Timing data in future studies to correlate shock position and fluctuation with actual stagger angles of individual blades.

Acoustic facility resonance

In the study mentioned above, it was also found that the asymmetry in the circumferential shock pattern interacts with a planar acoustic mode, which evolves in the exhaust system of the facility for all transonic operating conditions near the stability limit (see sketch in Fig. 11a)). For the fan analyzed in [32] modal oscillations started to rise some hundred revolutions before rotating stall occurred. An amplification between asymmetric shock pattern and acoustic mode resulted in the initiation of a single stall cell and thus limited the stable operating range.

The frequency of this mode is around 14 Hz for all operating

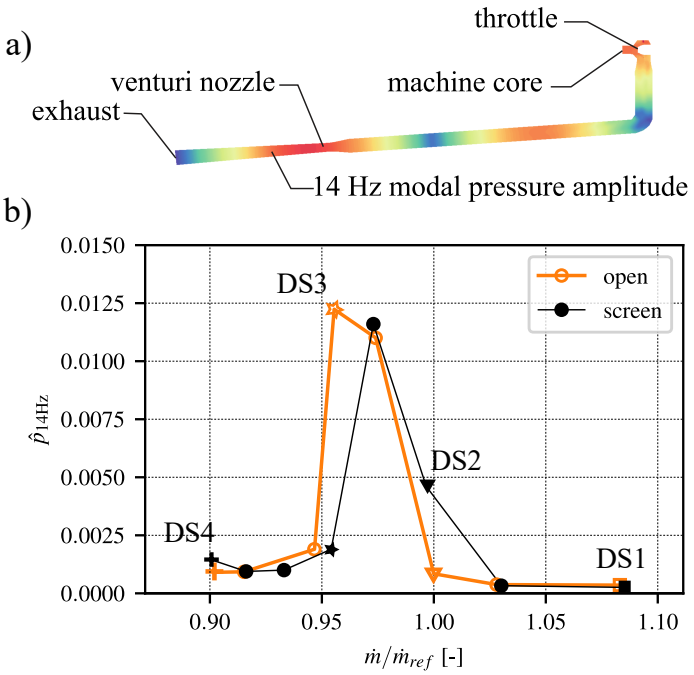

FIGURE 11: AMPLITUDE OF PLANAR ACOUSTIC DUCT MODE (14 HZ) OVER MASSFLOW

conditions near design speed. It has been shown that this frequency depends on the acoustic properties of the facility, namely the length of the exhaust system and the speed of sound.

To analyze the occurrence of the 14 Hz acoustic mode, a WPT in the stage intake has been used. Fig. 11b) shows the amplitude of the 14 Hz pressure fluctuation over the massflow range of operability measurements for both configurations. The graph has been obtained by performing a FFT with a Hanning-Window with a window size of 120 rotor revolutions (frequency resolution $\approx$ 1 Hz) and averaging the 14 Hz amplitude over all windows for each operating point individually.

In contrast to the study by Brandstetter et al. [32], who investigated a fan with a higher tip speed, it can be seen in Fig. 11b) that the acoustic mode develops for both configurations only for intermediate massflows slightly lower than design massflow. At higher and at lower massflow rates amplitudes diminish rapidly and thus the acoustic mode does not influence the stability limit for the rotor investigated here.

The comparison of open and screen configuration reveals a shift of maximum 14 Hz amplitude to lower massflows, if the TCS is not installed in front of the facility. It is remarkable that the maximum reached amplitude is nearly identical for both configurations. Hence, the TCS affects the onset of the acoustic duct-mode, shifting it towards higher massflow but the maximum amplitude remains constant.

Unsteady aerodynamics

The unsteady aerodynamics of the blade tip flow i.e. the frequency content of the flow field in this region, can be investigated by regarding spectra of the WPT above the LE in Fig. 12. The presented mean spectra are obtained by normalizing the raw pressure signal with the total pressure at the stage intake, calculating a FFT with a Hanning-window with a window size of 40 rotor revolutions and averaging all windows for each operating point respectively. In order to isolate non-synchronous pressure fluctuations an ensemble average of 20 revolutions is subtracted from the signal before the FFT is calculated. The spectra for OP_{DS1} are not shown here, because they are nearly identical for both configurations and no remarkable peaks are visible.

Corresponding to Fig. 11, a peak at 14 Hz ($<$ EO 0.1) is visible for the screen configuration in the spectrum of OP_{DS2} and for the open configuration at OP_{DS3} respectively. Due to a modulation of this frequency at the rotor blades, strong peaks around the BPF are visible for the configuration, for which the 14 Hz peak is observed. In addition, scattering of the acoustic mode causes sidebands around the BPF with distances of multiple integer EO (see [33] for details). Besides these differences at OP_{DS2} and OP_{DS3} related to the acoustic mode, it is noticed that noise levels are identical for both configurations.

This similarity can be observed at the highly throttled operating point OP_{DS4} as well. The reduction in massflow from OP_{DS2} to OP_{DS4} results in rising noise levels and in the formation of a broadband hump around EO 8. This broadband hump denotes the presence of convective disturbances as described by Rodrigues et al. [28] and Brandstetter et al. [33].

Aeroelastic behavior

The mechanical behavior of the rotor blades at different operating points can be analyzed by regarding the spectra of a representative blade mounted strain gauge shown in Fig. 13. The spectra have been calculated using the same parameters as the WPT spectra presented in Fig. 12 and are normalized with the maximum amplitude of the screen configuration at OP_{DS4}. In contrast to the spectra shown above, the ensemble average was not subtracted here. This allows a comparison of synchronous vibration amplitudes in addition to the analysis of non-synchronous vibrational frequencies.

In Fig. 13 the broadband vibration levels as well as the eigenmode vibration amplitudes differ only slightly between both configurations at the shown operating points.

In contrast to that the strain gauge spectra show significantly higher vibration amplitudes at integer engine orders below EO 7 for the open configuration. These strong blade vibrations with low integer EO frequencies can be explained by the observed differences in inflow conditions in Fig. 6 and 7. As described in the previous section, the static pressure profile upstream of the rotor is strongly asymmetric around the circumference and con-

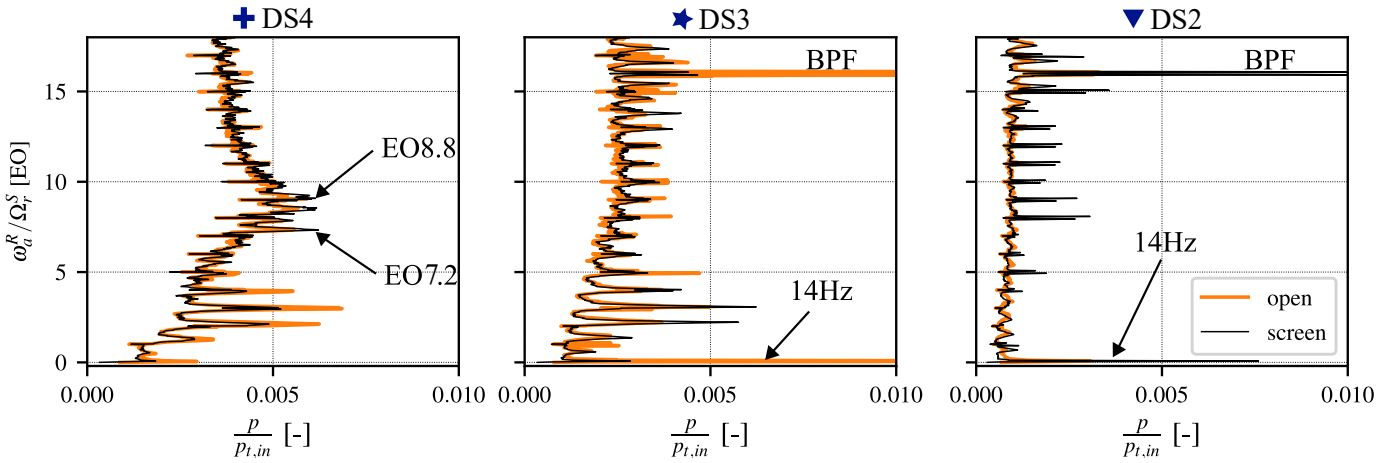

FIGURE 12: SPECTRA OF WPT ABOVE LE AT DIFFERENT OPERATING POINTS AT DESIGN SPEED, ENSEMBLE AVERAGE SUBTRACTED

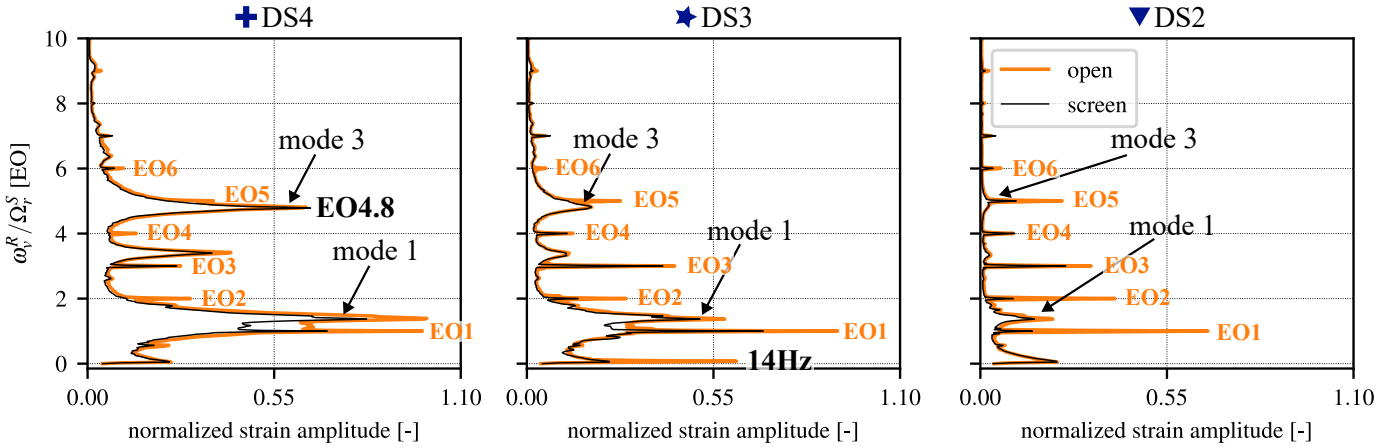

FIGURE 13: SPECTRA OF REPRESENTATIVE BLADE-MOUNTED STRAIN GAUGE AT DIFFERENT OPERATING POINTS DESIGN SPEED

sists of several mode orders for the open configuration. These mode orders are fixed in the non-rotating frame of reference and represent therefore a periodic disturbance in the rotating frame of reference. Thus, they force the rotor blades to vibrate with frequencies, which are integer multiples of the rotor speed Ω_r^S. At the last stable operating point OP_{DS4} the amplitudes of these synchronous vibrations, especially those with a frequency of EO 1, are of the same order of magnitude as the amplitudes of the first eigenmode. This indicates that the synchronous vibrations are not at all negligible.

In the screen configuration the circumferential asymmetry i.e. the inflow inhomogeneity of the static pressure profile is strongly reduced, resulting in a strong reduction of synchronous vibration amplitudes of nearly all EO frequencies below EO 7.

Besides these differences the comparison of the strain gauge spectra for both configurations at OP_{DS3} depicts a peak at 14 Hz for the open configuration. This vibration is attributed to the occurrence of the planar acoustic mode for the measurement without TCS at this operating point. As observed above, this mode is not present at the representative operating point for the screen configuration. In contrast to that, at OP_{DS2} a 14 Hz peak should be present in the strain gauge spectrum for the screen configuration, as the acoustic duct mode is clearly visible in the corresponding WPT spectrum. But due to the lower amplitude of the 14 Hz pressure fluctuation compared to the open configuration at OP_{DS3}, the corresponding vibration amplitude is lower as well and is hidden between broadband vibration below EO 0.5.

The rising amplitudes of the third eigenmode can be explained by comparing the strain gauge spectra in Fig. 13 to the WPT spectra in Fig. 12. Within the mentioned broadband hump around EO 8, which is visible at OP_{DS4} in the WPT spectra of both configurations, distinct frequency peaks at EO 7.2 and EO 8.8 establish. These peaks indicate the presence of convective disturbances with nearly constant propagation speed in the stationary frame of reference, which is determined by the aerodynamics of the mean flow [33]. Rodrigues et al. [28] have shown that it lies within 55 and 60 % of the rotational speed for the fan investigated here, what corresponds to a propagation velocity of

$$\frac{\Omega_a^R}{\Omega_r^S} = \frac{\Omega_a^S}{\Omega_r^S} - 1 = -0.4 \text{ to } -0.45 \tag{4}$$

in the rotating frame of reference. When the rotor is throttled towards the stability limit, a lock-in of these convective disturbances with the structural eigenmode with the eigenfrequency $\omega_{v,lock} = 4.8$ in the rotating frame of reference occurs. Due to the lock-in the global propagation speed Ω_a^R is slightly adjusted, so that the resonance condition

$$\omega_{v,lock} = \omega_{a,lock} = N_a \Omega^R_{a,lock} \tag{5}$$

is fulfilled with an integer aerodynamic wave number of $N_a = -12$. The necessity of matching inter-blade phase angles of the aerodynamic wave φ_a and the vibration pattern φ_v

$$\varphi_v = \varphi_a \longrightarrow N_v \equiv N_a \pmod{N_b} \tag{6}$$

results in an aliased structural nodal diameter equal to $N_v = 4$, because N_a is greater than $0.5 \cdot N_b$, where N_b is the number of rotor blades [34].

From Fig. 13 it is evident that vibrations in the third eigenmode can already be observed at O_{DS2} and OP_{DS3} for both configurations, but with lower amplitude as at OP_{DS4}. To compare the evolution of NSV for both configurations quantitatively, Fig. 14 shows the amplitudes of the structural vibration and the corresponding pressure fluctuation amplitudes depending on the massflow for all operating points of the operability measurements.

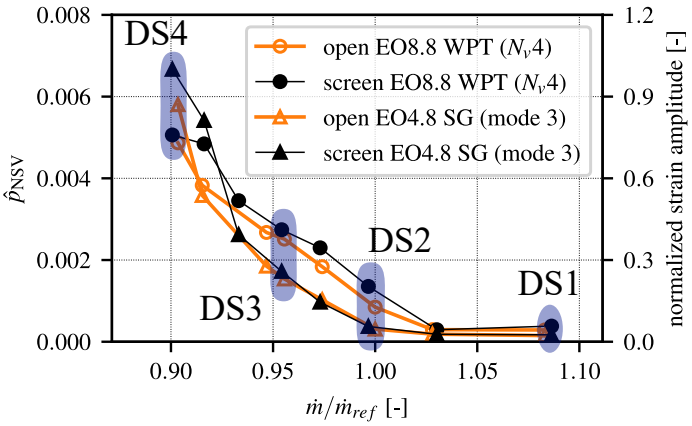

FIGURE 14: EVOLUTION OF NSV RELATED AMPLITUDES: EO4.8 - THIRD EIGENMODE; EO8.8 - PRESSURE FLUCTUATION N_V 4

In Fig. 14 the amplitudes of the pressure fluctuations with EO8.8 (and EO7.2 respectively) start to rise at higher massflows than the amplitudes of the third eigenmode vibration for both configurations. This confirms the findings in Brandstetter et al. [35], where small vortical disturbances are detected long before the stability limit is reached. They travel around the circumference until a lock-in with a blade eigenfrequency occurs and vibration amplitudes start to rise.

The comparison of both configurations shows slightly higher pressure fluctuation amplitudes at all operating points for the screen configuration and as well slightly higher vibration amplitudes at the two operating points with the lowest massflow. This indicates a reduced NSV amplitude for the open configuration, however, the graphs presented in Fig. 14 show that the evolution over massflow is comparable. Further studies will be necessary to clarify, if steady inflow inhomogeneity reduces the tendency towards NSV.

In addition, this similarity of NSV behavior between both configurations proves that synchronous and non-synchronous vibrations are linearly superimposed and do not influence each other in the presented measurement setup. This is yet challenging for experiment conduction, as real-time mode decomposition is necessary for surveillance measurements to distinguish between eigenmode vibration and synchronous vibration.

The investigations described above revealed differences as well as similarities between both configurations at design speed. The similarities concerning asymmetric shock pattern around the circumference, unsteady aerodynamics at the blade tip and NSV confirm a negligible influence of the TCS on these phenomena. In contrast to that, strong inhomogeneity in inflow conditions forces the rotor blade to vibrate with low integer EO frequencies in the open configuration, which can not be neglected as they occur at the same amplitude level as critical non-synchronous vibrations.

PART SPEED

In this section a selection of the investigations presented above are conducted for the part speed line, in order to characterize the influence of the TCS is this regime and provide a more global picture.

As described above, Fig. 9b) visualizes the ensemble averaged part speed flow field above the blades for the screen configuration, where the rotor works subsonic. In accordance to design speed line findings, reducing the massflow leads to a reduction of the axial velocity, which can be seen in a smaller low pressure region near the LE at OP_{PS3} compared to OP_{PS2} and OP_{PS1}. In contrast to the design speed operating points, the circumferential asymmetry at throttled operating points is much weaker at part speed. Thus, differences between screen and open configuration are even smaller at this rotational speed and it is concluded that the TCS has no influence on the ensemble averaged blade tip flow field at the respective circumferential sensor position (336°).

In order to analyze unsteady aerodynamics, Fig. 15 presents the spectrum of the WPT above the LE for the configurations with and without TCS at OP_{PS2}, which is representative for the whole part speed line. The mean spectra are calculated in the same way as those for design speed and the ensemble average has been subtracted. In Fig. 15 marginal differences in broadband noise level for both configurations are observed. Significant differences are only visible in the low frequency range and around the BPF (the BPF peak itself is not visible due to subtraction of the ensemble average). The peak in the low frequency range below EO0.1, which is only visible for the open configuration, has a higher peak width as the 14 Hz peak at design speed.

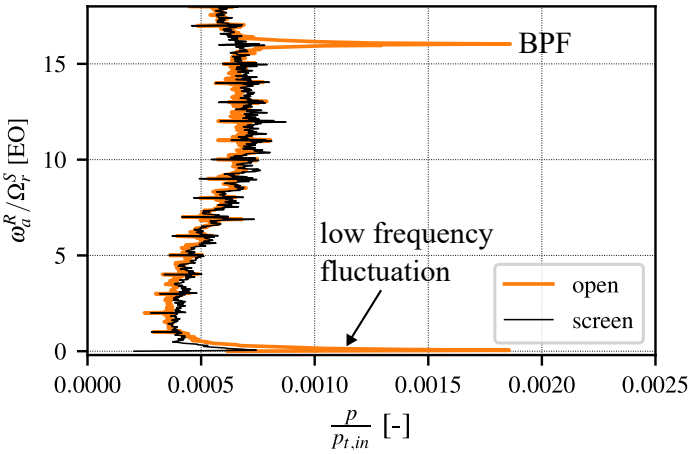

FIGURE 15: SPECTRA OF WPT ABOVE LE AT OP_{PS2} (PART SPEED), ENSEMBLE AVERAGE SUBTRACTED

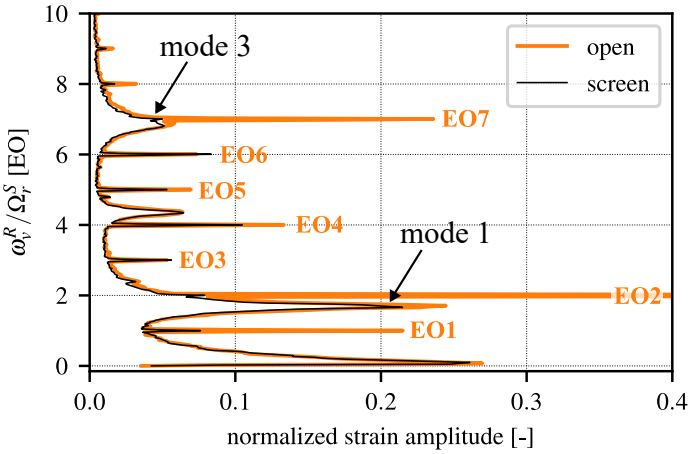

FIGURE 16: SPECTRA OF REPRESENTATIVE BLADE MOUNTED STRAIN GAUGE OP_{PS2} (PART SPEED)

This indicates that this peak is related to a broadband, low frequency disturbance.
The frequency peak around the BPF has the same amplitude as the low frequency peak for the open configuration and is caused by a modulation of the low frequency disturbance at the rotor blades. To further investigate this phenomenon, enhanced flow field measurements in the upstream region, combined with Particle Image Velocimetry (PIV) measurements in the rotor section are envisaged for future investigations.
As already mentioned above, the spectra of OP_{PS2} are representative for the part speed line, i.e. the phenomena observed here, are present at OP_{PS1} and OP_{PS3} as well.

To compare the mechanical behavior of the rotor blades at part speed, Fig. 16 shows the mean spectra of one representative blade mounted strain gauge (the same which has been used for design speed) at OP_{PS2}, calculated with the same parameters as for design speed. As above, and in contrast to the WPT spectra, the ensemble average has not been subtracted here.
The spectra in Fig. 16 show identical broadband vibration amplitudes over the whole frequency range as well as nearly identical peak amplitudes for the eigenmodes. In contrast to this similarity, Fig. 16 reveals significantly higher integer EO vibration amplitudes for the open configuration below EO 7, which again can be explained with the different inflow conditions in both cases. Thus, these observations fit perfectly to those in the design speed section and confirm a global characterization of the influence of the TCS over the whole operating range.

CONCLUSION

In the presented study, the influence of a TCS on the aerodynamic and aeroelastic behavior of a modern composite low-speed UHBR fan stage has been investigated experimentally. In order to characterize the underlying physical phenomena a back-to-back comparison of measurements with and without TCS at different operating points at two different speed lines is presented.

The comparison of inflow conditions for both configurations revealed significant differences concerning circumferential inhomogeneity and unsteadiness of the flow field upstream of the rotor. For the open configuration the static pressure profile around the circumference in the stage intake is composed of different circumferential mode orders while it has a pure sinusoidal shape with mode order 1 in the case of the screen configuration. The interaction of this asymmetric pressure profile with the rotor results in strong synchronous vibrations at all investigated operating points at design and part speed. In the screen case inflow conditions are more homogeneous and synchronous vibration amplitudes are significantly reduced.

Besides this remarkable difference, the investigation showed a negligible influence of the TCS on steady and unsteady aerodynamics in the blade tip region including aerodynamic flow features like shock strength and distribution. The aeroelastic behavior of the rotor blades at non-synchronous vibrational frequencies was found to be in good agreement for both configurations, too. It is remarkable that NSV, which is the stability limiting phenomenon, develops for both configurations in the same way and is linearly superimposed to synchronous vibrations in the presented setup. This results in a comparable stable operating range of both configurations.

The detailed aerodynamic and aeroelastic characterization of the influence of the TCS presented in this study provides insight into physical mechanisms and complements the acoustic investigations, which had been carried out in the past. Therefore it closes the gap of knowledge in literature concerning aerodynamic and aeroelastic effects of a TCS and serves as a basis for the design of experiments for future measurement campaigns.

ACKNOWLEDGMENT

The presented research was supported through the European Union's Seventh Framework Programme for research, technological development and demonstration, ENOVAL, grant agreement N604999

and the Clean Sky 2 Joint Undertaking (JU) under grant agreement N864719, CATANA. The JU receives support from the European Union's Horizon 2020 research and innovation programme and the Clean Sky 2 JU members other than the Union. The paper reflects only the author's view and the JU is not responsible for any use that may be made of the information it contains. Assessment of the test facility was enabled through financial supports of Agence Nationale de la Recherche (ANR, Project d'EqupEx PHARE) and Conseil pour la Recherche Aeronautique Civile (CORAC - Programme CUMIN). Buildings and infrastructure were supported by ECL, instrumentation supported by Institut Carnot (INGENIERIE@LYON - Project MERIT). We are grateful for the continuous collaboration and financial support of SAFRAN AE since the beginning of this project and specifically for the present measurement campaign. The authors would like to particularly acknowledge the precious contributions of Gilbert Halter, Lionel Pierrard, Pierre Laucher and Sebastien Goguey.

NOMENCLATURE

BPF	Blade Passing Frequency
DS	Design Speed
ECL	Ecole Centrale de Lyon
EO	Engine Order
FFT, FT	(Fast) Fourier Transformation
ICD	Inflow Control Device
JU	Joint Undertaking
$\dot{m}$	massflow
N_a	aerodynamic wave number (circumferential mode order)
N_v	structural Nodal Diameter
N_b	number of rotor blades
NSV	Non Synchronous Vibrations
LE	Leading Edge
OP	Operating Point
p	pressure
PIV	Particle Image Velocimetry
PS	Part Speed
SAE	SAFRAN Aircraft Engines
TCS	Turbulence Control Screen
TE	Trailing Edge
WPT	Wall Pressure Transducer
θ	circumferential position
Π_t	Total Pressure Ratio
σ	standard deviation
φ	inter-blade phase angle
Ω_r^S	angular velocity of the rotor
Ω_a^S	propagation velocity of convective disturbance
ω_a^S	angular frequency of pressure fluctuation
ω_v^R	angular vibration frequency

REFERENCES

[1] Cumpsty, N. A., and Lowrie, B. W., 1974. "The Cause of Tone Generation by Aero-Engine Fans at High Subsonic Tip Speeds and the Effect of Forward Speed".

[2] Feiler, C., and Merriman, J., 1974. "Effects of forward velocity and acoustic treatment on inlet fan noise". In 6th Aircraft Design, Flight Test and Operations Meeting, p. 946.

[3] Roundhill, J., and Schaut, L., 1975. "Model and full scale test results relating to fan noise in-flight effects". In 2nd Aeroacoustics Conference, p. 465.

[4] Filleul, N. L. S., 1966. "An investigation of axial flow fan noise". *Journal of sound and vibration, 3*(2), pp. 147–165.

[5] Mani, R., 1971. "Noise due to interaction of inlet turbulence with isolated stators and rotors". *Journal of Sound and Vibration, 17*(2), pp. 251–260.

[6] Hanson, D. B., 1974. "Spectrum of rotor noise caused by atmospheric turbulence". *The Journal of the Acoustical Society of America, 56*(1), pp. 110–126.

[7] Hodder, B. K., 1974. "The effects of forward speed on fan inlet turbulence and its relation to tone noise generation".

[8] Shaw, L., Woodward, R., Glaser, F., and Dastoli, B., 1977. "Inlet turbulence and fan noise measured in an anechoic wind tunnel and statically with an inlet flow control device". In 4th Aeroacoustics Conference, p. 1345.

[9] Cocking, B., and Ginder, R., 1974. "The effect of an inlet flow conditioner on fan distortion tones". In 4th Aeroacoustics Conference, p. 1324.

[10] Lowrie, B., and Newby, D., 1977. "The design and calibration of a distortion reducing screen for fan noise testing". In 4th Aeroacoustics Conference, p. 1323.

[11] Gedge, M. R., 1980. "A design procedure for fan inflow control structures". *NASA CR-165625, September*, pp. 81–96.

[12] Atvars, Y., and Rogers, D., 1980. "The development of inflow control devices for improved simulation offlight noise levels during static testing of a HBPR turbofan engine". In 6th Aeroacoustics Conference, p. 1024.

[13] Woodward, R. P., and Glaser, F. W., 1981. "Effect of inflow control on inlet noise of a cut-on fan". *AIAA Journal, 19*(3), pp. 387–392.

[14] Peracchio, A. A., 1982. "Assessment of inflow control structure effectiveness and design system development". *Journal of Aircraft, 19*(12), pp. 1045–1051.

[15] Preisser, J. S., and Chestnutt, D., 1984. "Flight effects on fan noise with static and wind-tunnel comparisons". *Journal of aircraft, 21*(7), pp. 453–461.

[16] Homyak, L., McArdle, J., and Heidelberg, L., 1983. "A compact inflow control device for simulating flight fan noise". In 8th Aeroacoustics Conference, p. 680.

[17] Rademaker, E., Sijtsma, P., and Tester, B., 2001. "Mode detection with an optimised array in a model turbofan engine intake at varying shaft speeds". In 7th AIAA/CEAS Aeroacoustics Conference and Exhibit, p. 2181.

[18] Mueller, D., Schulz, H.-J., Zitouni, G., and Baumann, W., 2005. "Europe's largest aero acoustic test facility for aero engine fans-the development and operation of the anecom aerotest anechoic chamber". In 11th AIAA/CEAS Aeroacoustics Conference, p. 3050.

[19] Khaletskiy, Y., Mileshin, V., and Shipov, R., 2008. "Acoustic test facility for aero engine fans". *Journal of the Acoustical Society of America, 123*(5), p. 3249.

[20] Schulz, H.-J., and Köhler, W., 2011. "UFFA - Universal Fan Facility for Acoustics, An Enhancement of Europe's Largest Aero Acoustic Test Facility for Aero Engine Fans". In inter.noise.

[21] Sturm, M., and Carolus, T., 2013. "Large scale inflow distortions as a source mechanism for discrete frequency sound from

isolated axial fans". In 19th AIAA/CEAS Aeroacoustics Conference, p. 2105.

[22] Funke, S., Siller, H. A., Hage, W., and Lemke, O., 2014. "Microphone-array measurements of a Rolls-Royce BR700 series aeroengine in an indoor test-bed and comparison with free-field data". In 20th AIAA/CEAS Aeroacoustics Conference, p. 3070.

[23] Behn, M., Pardowitz, B., and Tapken, U., 2018. "Separation of tonal and broadband noise components by cyclostationary analysis of the modal sound field in a low-speed fan test rig". In International Conference of Fan Noise, Aerodynamics, Applications and Systems, pp. 18–20.

[24] Caldas, L., Oertwig, S., Rudolphi, A., Meyer, R., Enghardt, L., and Tapken, U., 2019. "Development and assessment of an inflow control device and a bell-mouth for a low-speed aeroacoustic fan rig". In 25th AIAA/CEAS Aeroacoustics Conference, p. 2713.

[25] Köhler, W., 2012. "The Influence of the TCS on the Circumferential Mode Distribution in the Inlet of a Fanrig (UFFA)". In Turbo Expo: Power for Land, Sea, and Air, Vol. 44748, American Society of Mechanical Engineers, pp. 1813–1822.

[26] Grizewski, L., Behn, M., Funke, S., and Siller, H. A., 2021. "Cyclostationary Analysis of Fan Noise Influenced by an Inflow Control Device". *AIAA Journal*, pp. 1–12.

[27] Salze, E., Pereira, A., Souchotte, P., Regnard, J., Gea-Aguilera, F., and Gruber, M., 2019. "New modular fan rig for advanced aeroacoustic tests-Acoustic characterization of the facility". In 25th AIAA/CEAS Aeroacoustics Conference, p. 2603.

[28] Rodrigues, M., Soulat, L., Paoletti, B., Ottavy, X., and Brandstetter, C., 2020. "Aerodynamic investigation of a composite low-speed fan for UHBR application". In Turbo Expo: Power for Land, Sea, and Air, Vol. 84218, American Society of Mechanical Engineers, p. V10AT24A009.

[29] Brandstetter, C., Duquesne, P., Paoletti, B., Aubert, S., Ottavy, X., and Others, 2019. "Project PHARE-2—A High-Speed UHBR Fan Test Facility for a New Open-Test Case". *Journal of Turbomachinery, 141*(10).

[30] Wilson, M. J., Imregun, M., and Sayma, A. I., 2007. "The effect of stagger variability in gas turbine fan assemblies". *ASME Journal of Turbomachinery, 129*(2), pp. 404–411.

[31] Lu, Y., Lad, B., Green, J., Stapelfeldt, S., and Vahdati, M., 2019. "Effect of geometry variability on transonic fan blade untwist". *International Journal of Turbomachinery, Propulsion and Power, 4*(3), p. 24.

[32] Brandstetter, C., Paoletti, B., and Ottavy, X., 2019. "Compressible modal instability onset in an aerodynamically mistuned transonic fan". *Journal of Turbomachinery, 141*(3).

[33] Brandstetter, C., Ottavy, X., Paoletti, B., and Stapelfeldt, S., 2021. "Interpretation of stall precursor signatures". *Journal of Turbomachinery, 143*(12), p. 121011.

[34] Stapelfeldt, S., and Brandstetter, C., 2020. "Non-synchronous vibration in axial compressors: Lock-in mechanism and semi-analytical model". *Journal of Sound and Vibration, 488*, p. 115649.

[35] Brandstetter, C., Jüngst, M., and Schiffer, H.-P., 2018. "Measurements of Radial Vortices, Spill Forward, and Vortex Breakdown in a Transonic Compressor". *Journal of Turbomachinery, 140*(6), p. 61004.

The presented research was supported through the European Union's Seventh Framework Programme for Research, technological development and demonstration ENOVAL, grant agreement N604999 and the Clean Sky 2 Joint Undertaking (JU) under grant agreement N864719, CATANA. The JU receives support from the European Union's Horizon 2020 research and innovation programme and the Clean Sky 2 JU members other than the Union. This publication reflects only the author's view and the JU is not responsible for any use that may be made of the information it contains.

catana.ec-lyon.fr
christoph.brandstetter@ec-lyon.fr